Lab on a Chip

Micro- & nano- fluidic research for chemistry, physics, biology, & bioengineering
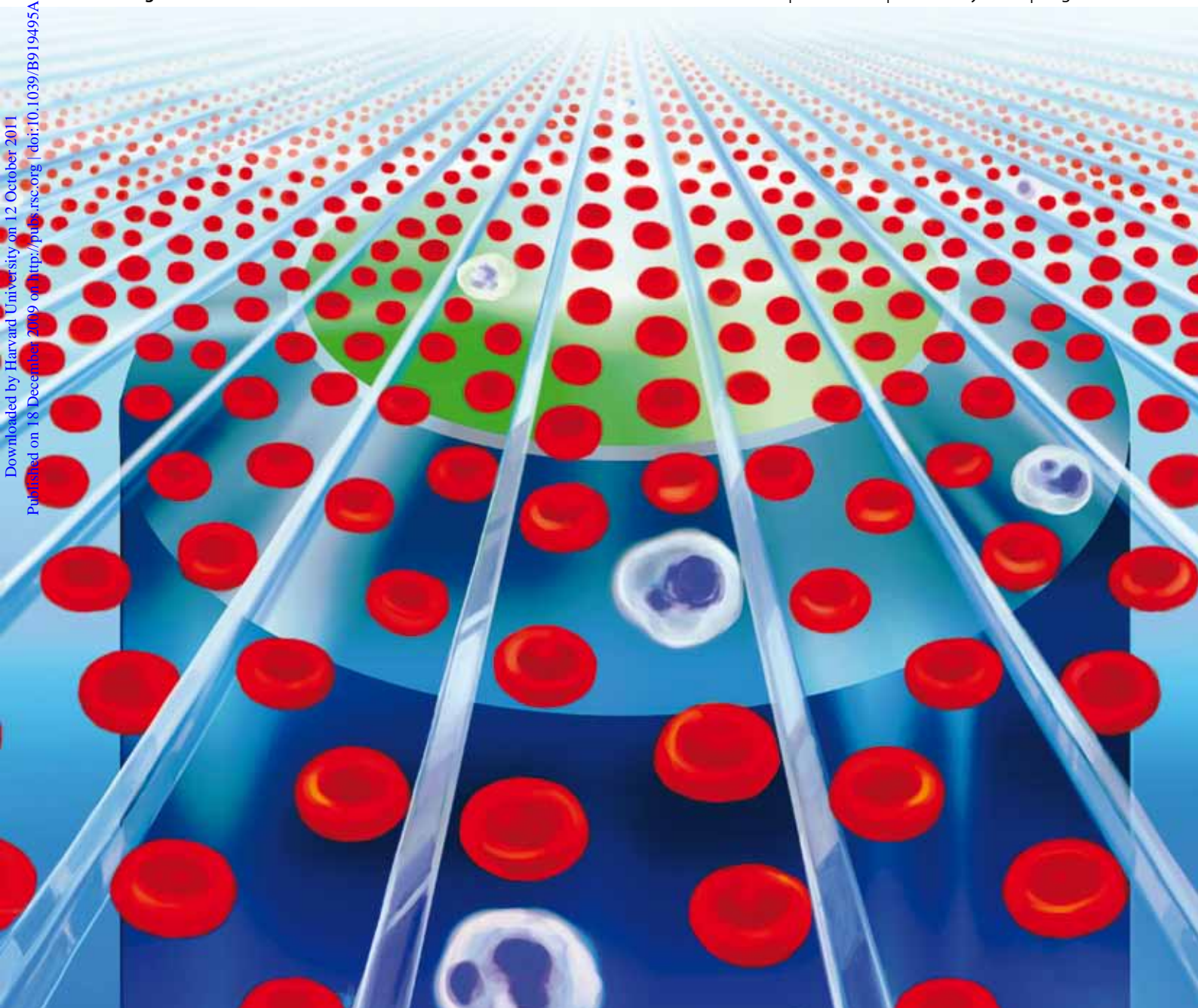
RSC Publishing

Di Carlo
Extreme throughput cytometry

Tovar-Lopez and Nesbitt
Platelet aggregation dynamics

Celebrating **10 Years** of publishing
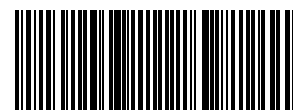
Sheathless inertial cell ordering for extreme throughput flow cytometry†

Soojung Claire Hur,[a] Henry Tat Kwong Tse[b] and Dino Di Carlo*[bc]

Rapid and accurate differentiation of cell types within a heterogeneous solution is a challenging but important task for various applications in biological research and medicine. Flow cytometry is the gold standard in cell analysis and is regularly used for blood analysis (*i.e.*, complete blood counts). Flow cytometry, however, lacks sufficient throughput to analyze rare cells in blood or other dilute solutions in a reasonable time period because it is an inherently serial process. In this study, we exploit inertial effects for label- and sheath-free parallel flow cytometry with extreme throughput. We demonstrate a microfluidic device that consists of 256 high-aspect ($W = 16$ μm, $H = 37$ μm) parallel channels yielding a sample rate up to 1 million cells s^{-1}, only limited by the field-of-view of our high-speed optical interrogation method. The particles or cells flowing through the channels are focused to one uniform z-position (SD $= \pm 1.81$ μm) with uniform downstream velocity ($U_{ave} = 0.208 \pm 0.004$ m s^{-1}) to reduce the probability of overlap and out-of-focus blur and provide similar cell signature images for accurate detection and analysis. To demonstrate a proof-of-concept application of our system operating at these throughputs, we conducted automated RBC and leukocyte counts on diluted whole blood and achieved high counting sensitivity and specificity (86–97%) compared to visual inspection of raw images. As no additional external forces are required to create ordered streams of cells, this approach has the potential for future applications in cost-effective hematology or rare-cell analysis platforms with extreme throughput capabilities when integrated with suitable large field-of view imaging or interrogation methods.

Introduction

Analysis of cells within a heterogeneous solution is a challenging but important task for various applications in biological research and medicine including general characterization of cellular protein content, identification of stem cells or tumor cells from dissociated tissue biopsies, and analysis of cell content in blood and other body fluids.[1] Among cell analysis techniques, flow cytometry is most commonly used because of the quantitative data and significant throughputs ($\sim$10 000 cells s^{-1}) achievable. Despite the current success of flow cytometry there is still interest in (1) further increasing throughput and (2) bringing the availability of instruments to the point-of-care. Clinically, flow cytometry is often used for blood analysis (*i.e.*, complete blood counts (CBCs)) to determine general patient health, blood diseases, and HIV or AIDS disease progression.[2,3] Today, a CBC test generally identifies subpopulations of white blood cells (WBCs), red blood cells (RBCs), platelets, hemoglobin, hematocrit volume, and platelet volume, but does not identify a variety of rare cells ($<$10 000 cells ml^{-1}) that can also be present in blood and potentially clinically useful (*e.g.* hematopoietic stem cells, endothelial progenitor cells, and circulating tumor cells). Statistically accurate identification of these cells is not possible in a reasonable time period using standard flow cytometry, especially in a background of 5×10^9 RBCs ml^{-1}, and even if RBCs are lysed to yield a background of $\sim$10^7 WBCs ml^{-1}. The limited throughputs possible in modern clinical benchtop flow cytometers and hematology analyzers are due to the serial nature of the cell focusing and interrogation process. For example the Abbott Cell-Dyn Hematology Analyzer relies on optical scattering and fluorescence intensity measurements for identification and enumeration of blood components based on a sheath-flow hydrodynamic focusing platform. Upon analysis the system requires sequential chemical lysis of WBC and RBC populations to achieve higher specificity. The complexity in cell interrogation and the use of consumable reagents required for operation prevent parallelization for increased throughput required for rare-cell detection purposes. There is also considerable interest in decreasing the cost of flow cytometry and hematology instruments. These systems have high fixed costs ($>$\$30 000), high operating costs (sheath fluids, lysis buffers), and lack of portability, which make them less than ideal for point-of-care or resource limited settings. Furthermore, in the United States, as required by the Clinical Laboratory Improvement Amendments (CLIA), the complexity of today's flow cytometers requires trained personnel to operate, analyze, and maintain the systems, further adding to operating costs. Thus a simpler system that would be eligible for CLIA waivers could reduce healthcare costs while also increasing patient access.

To address these challenges several efforts to miniaturize flow cytometry using microfluidic techniques have been previously explored such that costs are reduced, with the possibility of increased parallelization and throughput.[4–12] In most cases, the

[a]*Mechanical and Aerospace Engineering Department, University of California, Los Angeles, CA, 90095, USA*
[b]*Department of Bioengineering, University of California, Los Angeles, CA, 90095, USA. E-mail: dicarlo@seas.ucla.edu; Tel: +1 310 983 3235*
[c]*California NanoSystems Institute, Los Angeles, CA, 90095, USA*

† Electronic supplementary information (ESI) available: Supplementary figures (aspect ratio effects, development of inertial ordering, manual and automated image analysis); supplementary movies (massively parallel operation, unfocused and focused cells, change in z-positions); and MATLAB script for image analysis. See DOI: 10.1039/b919495a

macroscale mechanism of operation including "sheath flows" necessary to focus cells, and laser scatter and fluorescence are translated directly to the microscale with various miniaturization "tricks" employed to recapitulate the same macroscale performance. The apparent need for a robust, cost-effective, flow cytometer has resulted in numerous advances towards miniaturizing flow cytometry. The system demonstrated by Simonnet and Groisman operated at perhaps the highest rates, 17 000 cells s^{-1}, for cell counts which rely on three separate fluid inputs to create the "sheath-flow" necessary to focus cells to a single optically interrogated volume.[4] Similarly, the recent progress by Huang *et al.* explores an analogous technique by using a simpler design utilizing secondary flow around curving channels for sheath-based 3D hydrodynamic focusing to position cells to a single *z*-position.[5] They were able to achieve highly uniform cell positioning for WBC differentiation with a final throughput of 1700 cell s^{-1}. Golden *et al.* developed a microflow cytometer in which the sample fluid was ensheathed and hydrodynamically focused to small interrogated volume (20 × 34 × 30 μm^3) using a microstructured channel with chevron-shaped grooves.[6] Their cell interrogation utilized an embedded fiber-optic detection system allowing for miniaturization.

In contrast, other groups investigated sheathless microscale cytometer systems. Altendorf *et al.* demonstrated the ability to differentiate and count blood components in randomly dispersed flows.[7] Their design employed laser light scattering techniques achieving a 3-part WBC differentiation in addition to platelets and RBC enumeration with a throughput of 1000 cells s^{-1}. Recent work by Morgan *et al.* investigated sheathless cell counts in microchannel flows by using differential impedance spectroscopy for detection, allowing for WBC enumeration and sub-type differentiation, achieving a throughput of 100 cells s^{-1}.[8] An attempt at parallelization of optical cytometry techniques by Mckenna *et al.*, for the purpose of rare-cell detection, successfully resulted in a 384 channel parallel microfluidic cytometer capable of handling a large number of unique samples with a rare-cell sensitivity (~20 to 40 positive events in 1000 cells μl^{-1}).[9] Although successful for the application of identifying cells expressing parathyroid hormone receptor, the system's low-throughput (1070 cells s^{-1}), large footprint (25 × 50 cm^2), and complex confocal laser detection system may inhibit its adoption as a flow cytometer substitute. Further increases in throughput in these microscale systems have been challenging, mainly because the methods of cell focusing and optical interrogation are not trivially parallelized, and in the case of sheath-flow, require increased instrument bulk, minimizing the impact of the attempted miniaturization. It is apparent from this previous body of work that to have a commercially viable impact on rare-cell and point-of-care analysis, new systems will have to retain the accuracy but surpass the throughput of current benchtop systems while also being robust, cost-effective and easy to use (*i.e.* CLIA-waived). Thus there is an urgent need for developing fundamentally new methods to focus cells and collect data massively in parallel to meet these demands.

In this paper, we describe the device design, fabrication, and operation of a novel parallel microfluidic focusing mechanism and its experimental validation with high-speed image-based blood cell counts. The sheathless device is constructed with a single inlet splitting into 256 channels in which cells are positioned and spatially ordered by inertial effects to well defined focal planes in all parallel channels. The high uniformity in position and reduction in overlap of cells allows easier operation, detection and differentiation of cell types at higher cell concentrations than traditional flow cytometers. The device operates with 1% v/v diluted blood at an overall flow rate $Q = 2.5$ ml min^{-1} resulting in cell velocities of 0.42 m s^{-1} and total throughputs of ~28 million cells s^{-1}. Using conventional microscopic analysis and high-speed imaging of a 148 500 μm^2 field-of-view yields an analyzed throughput of ~1 million cells s^{-1} for 10 channels. With the capabilities of new wide-field imaging techniques[13] even higher throughputs can be expected. Thus, taking advantage of microscale physics, the presented technique provides improved throughput over traditional flow cytometry in a disposable platform with less logistical requirements, potentially enabling both rare-cell and point-of-care applications for flow cytometry.

Theoretical background

Inertial effects in microfluidic systems have recently been gaining much attention because of the ability to easily focus and order particles and cells continuously without external forces.[14] In brief, there are two inertial lift forces, namely a wall effect lift, F_{LW}, and a shear-gradient lift, F_{LS} (see Fig. 1b), inducing lateral migration of particles in confined flow and creating distinct inertial lift equilibrium positions at finite Reynolds number.[15] Moreover, it has been found that the critical channel length, L_f, that is required for particle focusing, can be calculated by balancing the shear-gradient lift force with Stokes drag.[14] L_f can be calculated as follows: $L_f = \pi \mu W^2 / \rho U_m a^2 f_L$, where W is the channel width in the direction of particle migration, μ and ρ are the fluid viscosity and density, U_m is the maximum channel velocity, a is the particle/cell diameter and f_L is the average lift coefficient that varies from 0.02 to 0.05 depending on the aspect ratio (H/W) from 2 to 0.5.[16]

In these finite-inertia channel systems, cells and particles in confined flow are observed to focus to distinct equilibrium positions corresponding with channel geometry.[17–20] Lateral particle migration to an annulus was first observed in centimetre scale pipes.[20] While particles flowing through square or rectangular channels were also found to focus to 4 distinct equilibrium positions corresponding to the channel fold symmetry (ESI, Fig. S1a†).[16,17,21,22] Increasing the channel aspect ratio removes unstable focusing positions at short faces and retains the two equilibrium positions centered at the long face of the channel[16,18,23] (ESI, Fig. S1b and c†).

Particles flowing in these channels also order in the direction of flow with preferred interparticle spacing[18,19,24,25] when the particle Reynolds number, $R_p = \rho U_m a^2 / \mu W$, is of order 1. This effect reduces particle overlap errors, important for flow cytometry applications.[17] The interparticle spacing has been observed in millimetre scale pipe flow as single trains[24] while in rectangular microchannels staggered double trains were found.[18] These observations were confirmed with simulations of cylinders flowing through infinite plates with finite Reynolds number.[19] Here we employ these high-aspect channels ($H/W > 2$), which focus particles to two positions with controlled interparticle
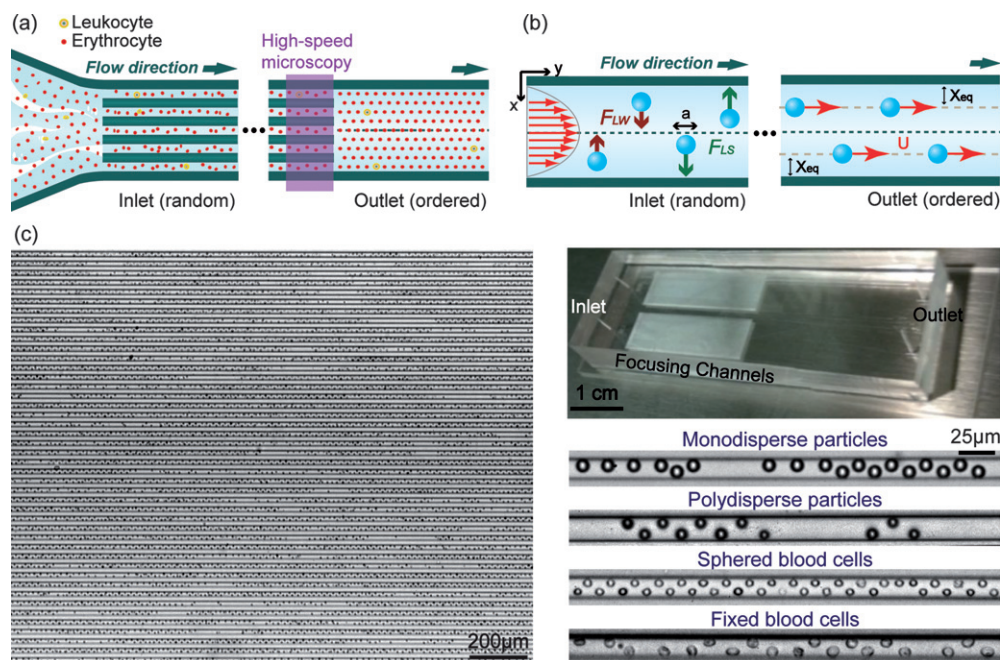
Fig. 1 Device working principle. The device consists of an inlet with a coarse filter, 256 parallel straight channels ($W = 16$ μm and $H = 37$ μm), a large reservoir, and an outlet. (a) Schematics describe an inlet where randomly distributed particles/cells were injected and an outlet where all injected particles/cells were uniformly spaced and flowing with uniform velocity. (b) Two lateral forces, namely wall effect lift, F_{LW}, and shear-gradient lift force, F_{LS}, that particles/cells with diameter, a, experience as they travel through the straight channel region induce lateral migration of particles and focus them at lateral equilibrium positions, X_{eq}, at the channel outlet, resulting in uniform particle velocity, U. (c) The photograph of the whole device and high-speed microscopic images of particles and blood cells flowing through the massively parallel inertial microfluidic device.

spacing and tight z-position for applications in sheathless flow cytometry.

Experimental methods

Device fabrication

The microfluidic chips with 256 parallel straight channels, whose individual channel width was 16 μm, were cast of PDMS (Sylgard 184, Dow Corning) using a photo-lithographically fabricated master mold. For mold fabrication, a 4″ silicon wafer was spin-coated with a 37 μm thick layer of a negative photo-resist (KMPR 1050, Microchem), exposed to UV-light through a designed Cr-photomask and developed. 80 g of PDMS base and crosslinker mixture were poured onto the mold and degassed for 30 min to remove all trapped bubbles. The degassed mold was then placed onto a leveled horizontal surface in a 65 °C oven for 3 h to complete the curing. The cured PDMS cast was separated from the mold and the inlet and outlet were punched with a pin vise (Pin vise set A, Technical Innovations Inc.). The punched PDMS chip was bonded to a slide glass by exposing both PDMS and slide glass surfaces to air plasma (Plasma Cleaner, Harrick Plasma) to enclose the microfluidic chip with 256 parallel channels and a reservoir.

Particle suspensions

Monodisperse polystyrene particles ($a = 9.9$ μm, Duke Scientific Corporation) were suspended in deionized water with 3% w/v Tween 80 (Fisher Chemical) to reach a final particle

concentration of 3% v/v. In addition, polydisperse polystyrene particles ($a_{ave} = 7.9$ μm, size distribution < 20% CV, Duke Scientific Corporation) were diluted to 1% v/v in the same Tween 80 solution.

Blood sample dilution and fixation

Whole blood samples were drawn from healthy volunteers into venous blood collection tubes (BD Vacutainer®) containing 0.4 ml of trisodium citrate (13.2 g l^{-1}), citric acid (4.8 g l^{-1}) and dextrose (14.7 g l^{-1}). Blood cells were suspended in Dulbecco's modified eagle's medium (DMEM) with 5% fetal bovine serum (FBS) to reach desired final cell concentrations. DMEM with 5% FBS will hereinafter be referred to as media. Both blood sample and media were placed in a water bath maintained at 37 °C for 30 min prior to mixing in order to minimize cell morphology changes. For the experiment with fixed blood cells, 1% v/v of glutaraldehyde (Fisher Scientific) was added to the diluted blood sample to polymerize live cells so that their shape is preserved.[26] After 15 min incubation, the fixed blood samples were washed three times with media to minimize formation of clumps of polymerized cells.

Sphering red blood cells

Red blood cells were isovolumetrically sphered (*i.e.*, initially biconcave discoid shaped red blood cells were modified to a spherical shape, by the addition of a trace amount of surfactant) to enhance the contrast between red blood cells and white blood cells for image analysis. Red blood cells were

sphered by following the recipe reported by Kim and Ornstein.[27] Sphering agent was prepared by dissolving 1 mg dl^{-1} sodium dodecyl sulfate in DPBS ($\sim$260 to 305 mOsm kg^{-1}). 80 µl of whole blood were mixed with 40 ml of sphering agent. The mixture was centrifuged at 2500 rpm for 3 min and the supernatant was aspirated to have final cell concentrations of 1 or 5% v/v.

Staining a blood smear

Blood samples were smeared and stained with Wright–Giemsa stain (Sigma-Aldrich, Accustain®) by following the standard staining protocol. In brief, smeared and thoroughly dried blood films on a slide were placed in Wright–Giemsa stain for 30 s and excessive stain was washed from the sample by placing the same slide in deionized water for 10 min without agitation. The slide was briefly rinsed in running deionized water followed by air drying before evaluation. The number of red and white blood cells was counted from microscopic images taken at randomly picked locations on the smeared sample and compared with the counting result from automated image analysis.

Massively parallel inertial focusing

The parallel ordering capability of the microfluidic chip was tested with mono/polydisperse polystyrene beads as well as diluted fresh, fixed or sphered whole blood samples. The solutions containing microparticles were injected into the device with a syringe pump (Harvard Apparatus, PHD 20000) to sustain an overall flow rate, Q, ranging between 5.5 µl min^{-1} and 2.5 ml min^{-1}. The loaded syringe was connected to 1/32 × 0.02″ PEEK tubing (Upchurch Scientific) by a ½″ luer stub (Instech Solomon) and tubing was secured in the punched inlet and outlet of the microfluidic device. It was possible to create well-ordered particle/cell streams evenly through more than 200 channels in parallel.

Uniform z-plane measurements of well-ordered particles

To verify that focused particles/cells were in the same z-plane, the monodisperse particle suspension was injected through a single straight channel with inverted aspect ratio (i.e., $W > H$ and $W : H \approx 2 : 1$). R_p was varied from 0.05 to 4.68 to determine the optimum condition yielding uniform z-positions.

High speed imaging

High-speed microscopic images of particle/cell trains were recorded downstream (see Fig. 1a) using a Phantom v7.3 high-speed camera (Vision Research Inc.) and Phantom Camera Control software. All high-speed images were taken using 1 µs exposure time and image intervals were varied according to the flow rate. Particle velocity and focusing position distribution were determined using high-speed microscopy and quantified manually using Irfanview. Obtained values were compared with those determined with the custom-built automated image analysis code implemented in MATLAB (see ESI, Fig. S3†) for validation.

Automated image analysis

The analysis of particle velocity, equilibrium position, total particle counts and red and white blood cell identification was performed post-experiment using a custom MATLAB script (see ESI† MATLAB script). Post-processing of the raw images included enhancing images with standard filtering techniques. The script allows users to define identification parameters such as size and matching intensity differential, in order to match to cell types of interest. A subset of the resulting data was then compared to measurements done manually to verify velocity and location accuracy (ESI, Fig. S3†). Additionally, the total red and white blood cell counts were manually examined to determine sensitivity (false negatives), the ratio of total identified to actual total, and specificity (false positives), the ratio of correctly identified to total identified.

Results and discussion

Key aspects required for successful implementation of inertial focusing for parallel cytometry applications include the ability to localize cells and particles to precise z-positions within a flow and ensure uniform velocities. The particles or cells are focused to one uniform z-position to reduce the probability of overlap and out-of-focus blur and provide similar cell signature images for accurate detection and analysis. A stable particle velocity is required such that each cell will have identical residence times within the given field-of-view yielding identical excitation intensities for laser based interrogation, or yielding the ability to synchronize the frequency of a raster scanning laser with cell downstream velocity. In the current work detection is solely based on size and contrast differences between cell types which limits its potential applications. However, the stable equilibrium position and particle velocity achieved would allow for future parallel fluorescence interrogation, holographic imaging, or dielectric characterization with appropriate integrated detection systems.

Uniform velocity and z-planes for inertially ordered particles

Previously it has been observed that, as the channel aspect ratio increases, particles in rectangular microchannels migrate predominantly to two lateral positions centered on the long channel faces[16,18,28] (see ESI, Fig. S1†). We employed this phenomenon to order particles/cells into precisely controlled lateral and vertical positions. Inertial focusing of spherical polystyrene particles and sphered red blood cells was stable (i.e., uniform cell signature images and travel velocity) after achieving overall flow rates of $Q = 1.2$ ml min^{-1} and 2.5 ml min^{-1}, respectively, corresponding to a consistent particle Reynolds number of $R_p = 1.22$ and 1.25, respectively. However, inertial focusing of discoid red blood cells, both fresh and fixed, was not completely stabilized even at flow rates as high as $Q = 2.5$ ml min^{-1}. Therefore, monodisperse polystyrene particles and sphered red blood cells were used for experiments evaluating the massively parallel inertial microfluidic system functionality (Fig. 1c and ESI, Movie 1†). High-speed microscopic images were obtained at 2.5 cm downstream, greater than the critical channel length, L_f, of 5 mm at the given flow rate (see ESI, Fig. S2†), ensuring complete particle ordering. The average

velocity of individual particles determined using manual image analysis was 0.208 ± 0.003 m s^{-1}, which falls within 0.1% of average particle velocity obtained from automated image analysis of 0.208 ± 0.004 m s^{-1} (see ESI, Fig. S3†). Fig. 1c illustrates that precisely ordered particle lattices travel through more than 200 parallel channels with uniform velocity, $U_{ave} = 0.208$ m s^{-1} (see Fig. 2). Using inverted aspect ratio channels (see Fig. 3a) as described in the methods, we observed that initially randomly distributed particles form well-ordered particle trains along the channel centerline (*i.e.* at the middle z-plane in our high-aspect ratio channels). Lateral equilibrium positions of focused particles, X_{eq}, were determined by both manual and automated image analysis and results agreed well within 1.37 ± 0.32 μm (see ESI, Fig. S3†). Fig. 3b and c illustrate the variation of particle focusing position in the z-direction as a function of particle Reynolds number, R_p. Initially randomly distributed particles began to migrate towards the channel centerline (*i.e.* a single z-plane) as R_p increased to 0.94. As the flow rate increased further ($R_p > 4.68$), however, particles started to occupy more than one z-plane focusing position, indicating that there is an optimum flow rate for inertial focusing yielding a single z-plane in high-aspect ratio channels (see ESI, Movie 3†). Reynolds number dependence and changes in particle equilibrium positions have also been observed in lattice-Boltzmann simulations of particle suspensions flowing through square ducts at high Reynolds number by Chun and Ladd.[21] Taking these data into account we limited further studies investigating focusing and analysis of blood cell populations to a flow regime yielding $R_p < 4.68$.

RBC and WBC counts

We next tested the effectiveness of the inertial ordering system's features: uniform (i) z-heights and (ii) velocities, towards accurate optical cell identification of RBCs and WBCs in blood without staining. This application was assisted by an automated MATLAB image analysis script to distinguish between RBCs and WBCs. Consequently, only large WBC types, neutrophils, eosinophils, basophils, and monocytes, were able to be identified
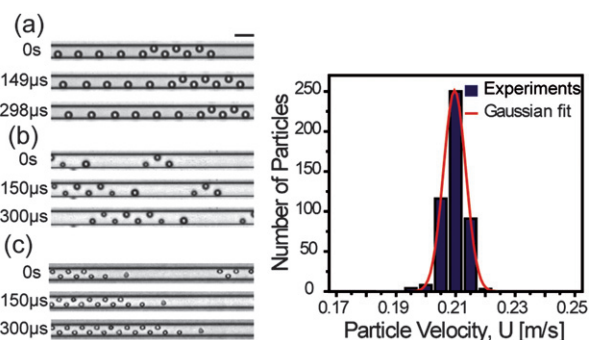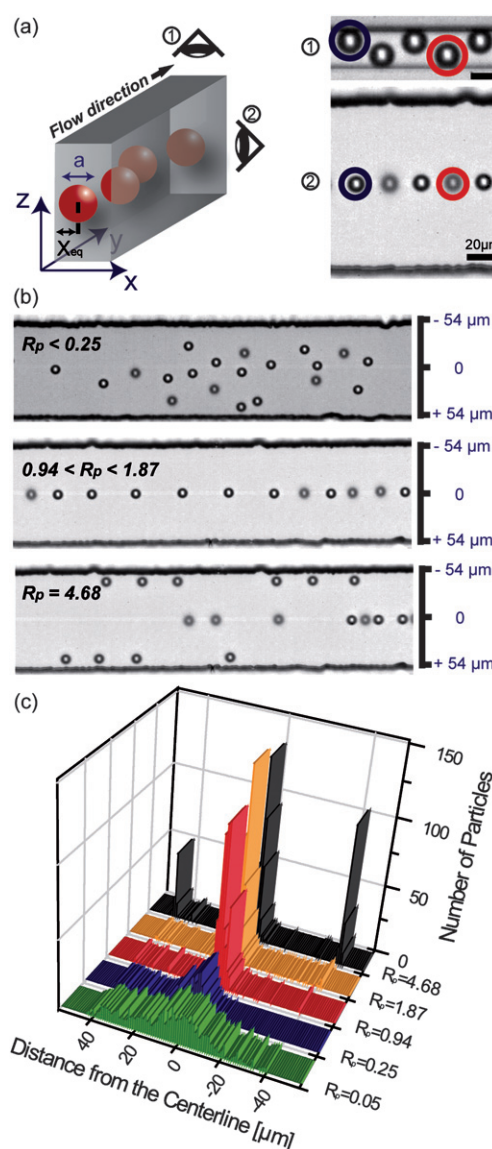

Fig. 3 Uniform z-plane for particles. (a) Schematic of inertial focusing of particles in a straight microfluidic channel with high-aspect ratio ($W : H = 1 : 2$) (left) and high-speed microscopic images obtained from two different viewpoints (right). (b) High-speed microscopic images and (c) 3D histogram illustrating flow speed dependence of particle alignment in the z-direction (viewpoint ②). At low flow rates, $R_p < 0.25$, flowing particles are randomly distributed while at moderate flow rates, $0.94 < R_p < 1.87$, particles aligned into a single train. As the flow speed exceeds the optimum flow rate, $R_p = 4.68$, particles begin to align at multiple focusing positions in the z-plane.

Fig. 2 Uniform velocity for particles/cells. Time-sequential high-speed microscopic images of focused (a) monodisperse polystyrene beads ($a = 9.9$ μm), (b) polydisperse polystyrene beads ($a_{ave} = 7.9$ μm), (c) 5% v/v sphered blood samples ($a_{ave} = 6.78$ μm). (d) Histogram illustrating velocity of monodisperse particles analyzed with the automated image analysis script ($U_{ave} = 0.208 \pm 0.004$ m s^{-1} with overall flow rate, $Q = 1.2$ ml min^{-1}, $R_p = 1.22$). Scale bar is 20 μm.

as the detection of each of the RBC and WBC types was based on visually distinguishable bright-field cell signatures (Fig. 4a and b). At the operational flow rate of 2.5 ml min^{-1} ($R_p = 1.25$), with a field-of-view of 10 of the 256 channels, we analyzed and determined the ratio of the partial WBC population to RBCs, and the sensitivity and specificity of RBC and WBC detection (see Table 1). A total count of $n = 7994$ RBCs and $n = 24$ WBCs resulted in a ratio of 0.25% WBCs to RBCs, this is within the same order of magnitude of the WBC to RBC ratio determined for the blood smear control, 0.10%. Both automated and control
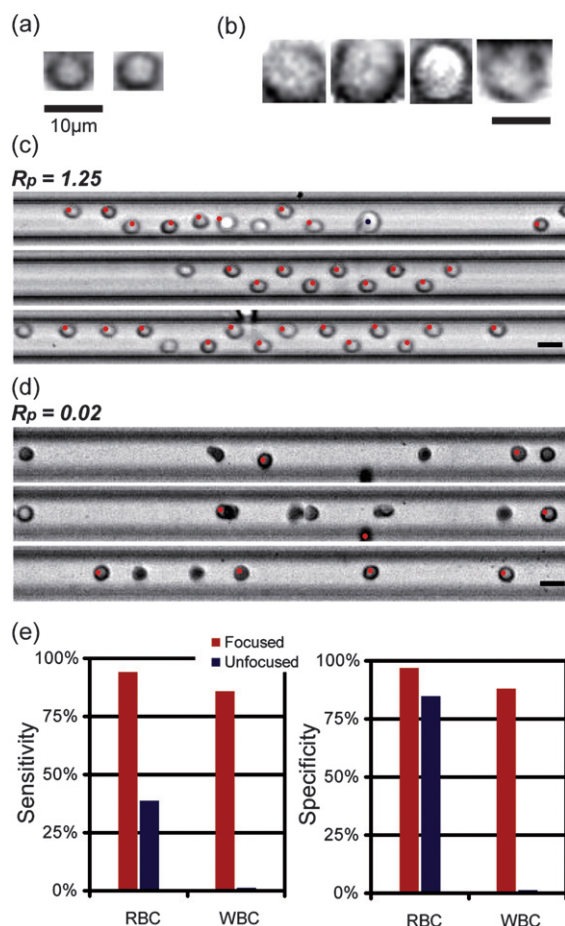
Fig. 4 Automated image analysis and detection using a custom script. Bright-field images used as kernels for (a) RBCs and (b) WBCs. (c) Focused and (d) unfocused detection, the RBCs and WBCs detected are marked with a red and blue dot, respectively. The unfocused cells are in multiple *z*-planes and overlap is apparent. (e) Comparison of detection sensitivity and specificity between focused and unfocused cells. Scale bars are 10 μm.

samples agreed well with reported literature values (∼0.07 to 0.23%).[29] Regarding the cell detection algorithm, the false positives—*i.e.* incorrect identification (<3% for RBCs and <12% for WBCs)—can largely be attributed to systematic errors such as defects in channel walls and cell clumping. Whereas the false negatives, cells evading detection (<6% for RBCs and <14% for WBCs), are contributed by an incomplete sphering process, or low cell image contrast due to cell membrane leakage.

In order to further examine the advantages of parallel inertial ordering and focusing to provide uniform cell conditions for optical interrogation we compared the automated cell identification accuracy in the focused system with cells in the same system that were unfocused due to a reduced flow rate of 50 μl min^{-1} ($R_p = 0.02$). At this low flow rate, the uniform array and focusing are lost and the cells are randomly dispersed throughout the *z*-plane as seen in *z*-plane measurements (see Fig. 4d and ESI, Movie 2†) along with high incidences of cell–cell overlap. These aspects significantly lowered ability to differentiate between RBCs and WBCs (Fig. 4d). The randomly dispersed out-of-plane cells evade detection and cell type identification due to a blurred cell signature. In addition, instances of cell–cell overlap are causes for undercounting and in some cases misidentification due to a false cell signature. Comparatively, inertial focusing operation increased sensitivity by 59%.

Although our blood counting accuracy and cell type differentiation capabilities fall short of the more complex commercial hematology analyzers, this system utilizes bright-field microscopy as its only interrogation method. Here simplicity, ease of use and robustness of automated enumeration and differentiation of cell types with an acceptable accuracy are achieved. Future integration with next-generation wide-field imaging techniques[13] based on diffraction pattern recognition can be readily implemented as patterns are likely to be highly uniform due to inertial focusing of cells to a narrow focal plane and uniform velocities this system provides. Furthermore, integration with state-of-the-art imaging techniques allows further reduction in system cost compared to demonstrated high-speed image analysis. Future increases in accuracy and degree of cell type differentiation can be expected to rival and surpass commercial hematology analyzers.

Conclusions

Here we have successfully designed and characterized a high-throughput sheath-free cell positioning system that can be integrated with next-generation wide-field optical imaging techniques for extreme throughput flow cytometry, promising interrogation rates up to 1 million cell s^{-1}. We tested the system using standard bright-field high-speed microscopy with a 10 channel FOV, and conducted automated detection of RBCs and WBCs in blood with high sensitivity and specificity for each cell type, which was not achievable with unfocused cells. With the future implementation of larger FOV acquisition technologies new applications are possible, including fast total complete blood counts with limited logistical footprint, and statistically significant identification of rare cells enabled by the extreme throughput.

Table 1 Ratio of WBC to RBC, sensitivity, and specificity values per sample

Sample	Total detected			Sensitivity		Specificity	
	RBC	WBC	WBC/RBC ratio	RBC (%)	WBC (%)	RBC (%)	WBC (%)
Blood smear	15 125	15	0.0010	—	—	—	—
Sample #1	4896	14	0.0028	92	82	95	86
Sample #2	3098	7	0.0023	95	89	98	90
Total	7994	24	0.0025	94	86	97	88

Acknowledgements

References

1 A. Yen, *Flow Cytometry: Advanced Research and Clinical Applications*, CRC Press, Boca Raton, Florida, 2nd edn, 1989, vol. 1, ch. 9, p. 170.
2 A. Landay, B. Ohlsson-Wilhelm and J. V. Giorgi, *AIDS (London)*, 1990, **4**, 479–497.
3 S. Siena, M. Bregni, B. Brando, N. Belli, F. Ravagnani, L. Gandola, A. C. Stern, P. M. Lansdorp, G. Bonadonna and A. M. Gianni, *Blood*, 1991, **77**, 400–409.
4 C. Simonnet and A. Groisman, *Anal. Chem.*, 2006, **78**, 5653–5663.
5 X. Mao, S. C. Lin, C. Dong and T. J. Huang, *Lab Chip*, 2009, **9**, 1583–1589.
6 J. P. Golden, J. S. Kim, J. S. Erickson, L. R. Hilliard, P. B. Howell, G. P. Anderson, M. Nasir and F. S. Ligler, *Lab Chip*, 2009, **9**, 1942–1950.
7 E. H. Altendorf, E. Iverson, D. Schutte, B. H. Weigl, T. D. Osborn, R. Sabeti and P. Yager, *Proc. SPIE-Int. Soc. Opt. Eng.*, 1996, **2678**, 267–276.
8 D. Holmes, D. Pettigrew, C. H. Reccius, J. D. Gwyer, C. van Berkel, J. Holloway, D. E. Davies and H. Morgan, *Lab Chip*, 2009, **9**, 2881–2889.
9 B. K. Mckenna, A. A. Selim, F. R. Bringhurst and D. J. Ehrlich, *Lab Chip*, 2009, **9**, 305–310.
10 D. A. Ateya, J. S. Erickson, P. B. Howell, Jr., L. R. Hilliard, J. P. Golden and F. S. Ligler, *Anal. Bioanal. Chem.*, 2008, **391**, 1485–1498.
11 T. D. Chung and H. C. Kim, *Electrophoresis*, 2007, **28**, 4511–4520.
12 D. Huh, W. Gu, Y. Kamotani, J. B. Grotberg and S. Takayama, *Physiol. Meas.*, 2005, **26**, R73–R98.
13 T. W. Su, S. Seo, A. Erlinger and A. Ozcan, *Biotechnol. Bioeng.*, 2009, **102**, 856–868.
14 D. Di Carlo, *Lab Chip*, 2009, **9**, 3038–3046.
15 J. P. Matas, J. F. Morris and E. Guazzelli, *J. Fluid Mech.*, 2004, **515**, 171–195.
16 D. Di Carlo, J. F. Edd, K. J. Humphry, H. A. Stone and M. Toner, *Phys. Rev. Lett.*, 2009, **102**, 94503–94504.
17 D. Di Carlo, D. Irimia, R. G. Tompkins and M. Toner, *Proc. Natl. Acad. Sci. U. S. A.*, 2007, **104**, 18892–18897.
18 J. F. Edd, D. Di Carlo, K. J. Humphry, S. Koster, D. Irimia, D. A. Weitz and M. Toner, *Lab Chip*, 2008, **8**, 1262–1264.
19 T. Inamuro, K. Maeba and F. Ogino, *Int. J. Multiphase Flow*, 2000, **26**, 1981–2004.
20 G. Segre and A. Silberberg, *Nature*, 1961, **189**, 209–210.
21 B. Chun and A. J. C. Ladd, *Phys. Fluids*, 2006, **18**, 031704.
22 A. A. S. Bhagat, S. S. Kuntaegowdanahalli and I. Papautsky, *Phys. Fluids*, 2008, **20**, 101702–101704.
23 Y. W. Kim and J. Y. Yoo, *J. Micromech. Microeng.*, 2008, **18**, 065015.
24 J. P. Matas, V. Glezer, E. Guazzelli and J. F. Morris, *Phys. Fluids*, 2004, **16**, 4192–4195.
25 Y. Yan, J. F. Morris and J. Koplik, *Phys. Fluids*, 2007, **19**, 113305–113312.
26 M. Faivre, M. Abkarian, K. Bickraj and H. A. Stone, *Biorheology*, 2006, **43**, 147–159.
27 Y. R. Kim and L. Ornstein, *Cytometry*, 1983, **3**, 419–427.
28 D. R. Gossett and D. Di Carlo, *Anal. Chem.*, 2009, **81**, 8459–8465.
29 W. F. Ganong, *Review of Medical Physiology*, McGraw-Hill Medical Publishing, New York, NY, 22nd edn, 2005, ch. 27, p. 516.